

Large-scale parameterization of 3D building morphology in complex urban landscapes using aerial LiDAR and city administrative data



Bartosz Bonczak^a, Constantine E. Kontokosta^{b,*}

^a Center for Urban Science and Progress, New York University, United States

^b Dept. of Civil and Urban Engineering and Center for Urban Science and Progress, New York University, United States

ARTICLE INFO

Keywords:

LiDAR
DSM
Urban morphology
Building parameters
Urban environment
City Data

ABSTRACT

The form and function of the modern city are defined by the three-dimensional contours of the built environment. The morphology of the urban landscape has significant implications for a city's sustainability, efficiency, and resilience. With advancements in remote sensing, especially airborne Light Detection and Ranging (LiDAR), the potential exists to model urban topography at an unprecedented spatial resolution and granularity and extract previously unavailable characteristics of individual buildings. In this study, we demonstrate the application of point-based voxelization techniques to extract design parameters in complex urban environments at unprecedented scale using New York City, and its more than 1,000,000 buildings, as a test case. Covering approximately 800 km², we develop a 1 m² resolution Digital Surface Model (DSM) derived from aerial LiDAR point cloud data, together with city administrative records, to calculate building massing, height, volume, exposed surface area, and compactness ratios for every building in the City. The proposed scalable approach creates a significant opportunity for city administrators, urban planners, architectural engineers, and building designers to understand the relationship between urban morphology and a range of infrastructure and environmental systems.

1. Introduction

As the pace of urbanization continues to accelerate, many cities are developing at higher densities to meet the increasing demand for living and working space (Glaeser, 2011). Urban morphology - the three-dimensional form of the city - has significant implications for a city's sustainability, efficiency, and resilience. The continued vertical expansion of cities necessitates a data-driven understanding of the relationship between the three-dimensional urban form and critical infrastructure operations and quality-of-life measures. However, there are few sources of high resolution data on building volumes, heights, and envelopes at the city scale, particularly in dense urban environments. Existing 3D models, such as Google Earth, provide useful tools for visualization, but their application for analytical purposes is limited (Google, 2017). Other data sources, such as 3D CityGML models or OpenStreetMap data, while valuable, are primarily static or rely on user-provided information (Open Geospatial Consortium, 2018; OpenStreetMap contributors, 2018). With advancements in remote sensing the potential exists to model urban topography at an unprecedented spatial resolution and granularity. Given the significant computing capability and data processing needed to derive insight from

these data, however, few examples of building-specific, city-scale applications in dense, complex urban environments currently exist.

Many cities undertake periodic surveys to collect detailed building and land use characteristics about individual properties. Unfortunately, this approach to data collection is costly, time consuming, and suffers from significant limitations in data quality and reliability. In recent years, the decreasing cost of remote sensing technology and data storage enable new methods for collecting administrative data on buildings and infrastructure at scale. One example is Light Detection and Ranging (LiDAR) technology (Vosselman & Maas, 2010). Depending on the method of acquisition (terrestrial or airborne), it can provide three-dimensional representations of a given region with high resolution and accuracy. The airborne data acquisition approach is specifically of interest as a way to obtain a comprehensive topographic urban model at the city scale. It is particularly important in urbanized landscapes like New York City where the number and heterogeneity of building structures is exceptional. While studies have examined the use of LiDAR in urban environments, the size and complexity of New York City - characterized by large variations in building heights, shapes, and spatial orientations - creates non-trivial challenges to the accurate and computationally-efficient extraction of building and urban parameters.

* Corresponding author at: 370 Jay Street, 12th Floor, Brooklyn 11201, NY, United States.

E-mail addresses: bartosz.bonczak@nyu.edu (B. Bonczak), ckontokosta@nyu.edu (C.E. Kontokosta).

Several recent studies have explored the use of LiDAR data in cities. Technical aspects of urban LiDAR scanning are presented by Vosselman and Maas (2010), Wehr and Lohr (1999), and Haarap and Lato (2016). Specific LiDAR applications in urban areas include creating Digital Terrain Models (DTMs) for urban planning, building extraction, flood mapping, urban parameter calculations, transportation planning, viewshed analysis, solar energy planning, and architecture (Grindgis.com, 2015; Wehr & Lohr, 1999). A common application is urban feature extraction and estimation of various building measures, such as height distribution and floor-to-area ratio (FAR) (Dias, Bastos, Correia, & Vicente, 2006; Gonzalez-Aguilera, Crespo-Matellan, Hernandez-Lopez, & Rodriguez-Gonzalez, 2013; Santos, Rodrigues, & Tenedorio, 2013; Yu, Liu, Wu, Hu, & Zhang, 2010). Variations to this approach rest primarily with different techniques for interpolation and edge detection and the level of detail, from simple building footprint identification (Neidhart & Brenner, 2003), to more complicated three-dimensional modeling of individual buildings (Matei, Sawhney, Samarasekera, Kim, & Kumar, 2008; Poullis & You, 2009; Priestnall, Jaafar, & Duncan, 2000; Rottensteiner & Ch, 2012; Shiravi, Zhong, & Beykai, 2012; Wu et al., 2017b; Zhou & Neumann, 2008). Other relevant use cases include estimation of building population using census data combined with an Airborne Laser Scanning (ALS) model (Lwin & Murayama, 2011), visibility of public green areas from different floors and angles of a building (Yu et al., 2016), identification of local urban patterns (Wu et al., 2017a), or the calculation of heating demand based on building density (Neidhart & Brenner, 2003). A particular interesting study by Steadman, Evans, and Batty (2009) uses LiDAR data for London to empirically test the relationship between wall area and volume. Several studies attempt to analyze how building shapes and urban morphology impact variations in solar radiation (Yu, Liu, Wu, & Lin, 2009) as a component of practical applications to the identification of optimal locations for solar panel installations on building rooftops (Ahearn & Ahn, 2011; Carneiro, Morello, Ratti, & Golay, 2009; Center for Advanced Research of Spatial Information - CARSI, 2016).

It is also common to find ancillary data sets integrated with LiDAR data to improve the accuracy of the building extraction process. Examples include digital aerial imagery (Alhaddad, Roca, Burns, & Garcia, 2008; Gonzalez-Aguilera et al., 2013; Goodwin, Coops, Tooke, Christen, & Voogt, 2009; Zhou, Simmers, & Cheng, 2004) and combined ALS and Unmanned Aerial Vehicle (UAV) collection methods (Rebelo, Rodrigues, Tenedório, Goncalves, & Marnoto, 2015), or terrestrial laser scanning to obtain detailed facades (Truong Pacheco Hong, Laefer, Hinks, & Carr, 2013). While these studies provide interesting exploratory analyses, they are limited in their geographical extents (a single block to a neighborhood) and the complexity of the modeled environment. Attempts to model large parts of the city based on LiDAR scanning were described by Poullis and You (2009), which resulted in impressive and realistic reconstructions of the centers of Atlanta and Baltimore. Other ancillary datasets that can be of value are land use and demographic information, building footprints, and road networks (Lwin & Murayama, 2011; Neidhart & Brenner, 2003; Santos et al., 2013; Yu et al., 2010).

As the density of development in cities increases to meet the demands created by an urbanizing global population, reliable estimates of the vertical surface of building envelopes, understood as an outer shells of the buildings, can provide useful information to better understand thermal efficiencies and losses, energy consumption patterns, urban wind flow modeling, solar access and shading, and other aspects of urban physics. There are significant relationships between building form and building performance, across dimensions such as envelope characteristics, space utilization rates, and energy efficiency. Typically, energy efficiency is expressed as a ratio of energy use to building Gross Floor Area (Kontokosta, 2015; Kontokosta & Tull, 2017) without considering the physical form of the building as part of large-scale performance comparisons. However, as identified in the studies by

Pacheco, Ordez, and Martnez (2012) and Depecker, Menezo, Virgone, and Lepers (2001), building shape (expressed in its compactness or exterior or envelope surface area to volume ratio) is one of the main contributing factor to building energy performance, followed by building orientation, its envelope material, shading, implemented passive systems and glazing ratio. More in-depth analysis of prototypical buildings suggest a strong correlation between compactness and energy performance (Ourghi, Al-Anzi, & Krarti, 2007; Parasonis, Keizikas, & Kalibatiene, 2012). However, given the lack of high-resolution city-scale data on buildings, these studies rely on prototypical models to represent elements of the actual urban built environment.

This paper presents a method for the extraction and estimation of building form, massing and other physical parameters from aerial LiDAR point cloud data for a large-scale, heterogeneous, and high-density urban environment using point-based voxelization methods (Laine, 2013; Nourian, Gonçalves, Zlatanova, Ohori, & Vo, 2016; Truong Pacheco Hong et al., 2013). Using New York City as our testbed, we estimate and validate these measures for over 1,000,000 buildings across 780 km² using a 3.8 billion point cloud dataset integrated with various city administrative data. Our work focuses on the calculation of the two measures excluded from previous city-scale building modeling methodologies:

- Building compactness ratio - a measure of surface area to volume;
- Exposed surface area - total envelope surface area less vertical surfaces shared by more than one building.

When combined with other urban datasets, our method for a high spatial resolution volumetric map of the city and its buildings can provide additional insight on building performance, design, and massing for parameter extraction and urban modeling.

2. Data

Our methodology requires the integration and analysis of several large-scale datasets. The basis for the analysis is aerial LiDAR data from a flyover of New York City conducted in 2013. We combine the resultant point cloud data with city administrative property records and building footprint shapefiles to associate building objects with individual property data in order to extract building-specific physical and architectural parameters.

2.1. New York City LiDAR point cloud data

The subject aerial LIDAR scanning was carried out by the Woolpert company between August 5th and August 15th, 2013, for the United States Geological Survey (USGS) as part of its Coastal and Marine Geology Program's effort to rezone flood plains in the region after Hurricane Sandy on October 29, 2012. During the ten flyover missions, an ALS-70 sensor installed on a Cessna 402 collected approximately 3.8 billion points covering more than 780 km² of the five boroughs (Manhattan, Brooklyn, Queens, The Bronx and Staten Island) with a mean density of two points per square meter, generating 100 GB of data. The device used was a Leica ALS-70500 kHz Multiple Pulses in Air (MPiA) LiDAR sensor installed in a Leica gyro-stabilized PAV30 mount characterized by lateral and vertical accuracy of 7–16 cm and 5–38 cm, respectively. Data quality and accuracy calibration processes were performed by the Woolpert company. They compared raw point cloud data against multiple ground survey checkpoints for vertical and horizontal accuracy assessment. The RMSE for the former was estimated at 5.3 cm and less than 10 cm for the latter. The LiDAR data were classified for different surface types, processed and projected in UTM, Zone 18, North American Datum of 1983 (2011) and NAVD 1988, GEOID12A for the vertical datum. The data are provided in 509 indexed LAS files (USGS, 2014). The final product resulted in a detailed three-

dimensional picture of the complex landscape of New York City. Despite its great precision, working with such large, detailed, and highly partitioned data can be computationally greedy, especially when applied to city-scale analysis.

2.2. Building footprint shapefile

The building footprint dataset consists of perimeter extents for over one million buildings in New York City. It is provided in a shapefile format (.SHP) by the NYC Department of Information Technology & Telecommunications (DoITT). In addition to the location and shape of the outline of each building, it contains information on the building name, year of construction, height of the roof, ground elevation, number of floors (on the tax lot level), built code, and other physical and zoning attributes. Several of these characteristics were derived using a planimetric approach from the 2014 New York Statewide Flyover. Aerial imagery served as a basis for this dataset and was collected to support the generation of a 0.5 ft. (15.24 cm) Ground Sample Distance (GSD) in natural colour. Developed planimetric features meet American Society for Photogrammetry and Remote Sensing (ASPRS) class 1 for horizontal and class 2 for vertical accuracy specifications. The dataset captures all of the buildings with an assigned Building Identification Number (BIN) number or with well-defined walls and roof areas greater than 400 ft² (37.16 m²) and taller than 12 ft. (3.66 m) ([City of New York, 2017](#)). Height values were estimated photogrammetrically using a combination of stereo imagery, LiDAR, and TIN models. A bare earth LiDAR-derived Digital Terrain Model (DTM) was used to estimate a single value for ground elevation at the building centroid location. Regardless of the complexity of specific building shapes, the dataset provides just a single value for the maximum height of the property. The height of the building was generated as the difference between the highest measured point of the roof (excluding antennas and roof fixtures) and the estimated ground elevation. Other attributes, such as year of construction or modification, number of floors, and footprint area, among others, were extracted from other city databases such as Primary Land Use Tax Lot Output (PLUTO) and NYC Department of Buildings (DOB) datasets. Local identifiers, such as Borough, Block and Lot number (BBL) and BIN are provided to facilitate integration with other New York City administrative datasets. The dataset is available from 2015 and is updated periodically. The data are provided in State Plane New York Long Island (FIPS 3104) geographical projection using US feet as a distance unit ([City of New York, 2015, 2017; Reilly, 2014](#)). For the purpose of this study, in order to minimize the temporal discrepancy with LiDAR data we use the footprint dataset published in 2015. The database identifies 1,082,437 individual buildings, out of which 1,081,709 (99.93%) were constructed before 2014. [Table 1](#) provides basic statistics of relevant fields such as height of roof, footprint area, property ground elevation, and number of floors.

2.3. New York city Primary Land Use Tax Lot Output Data (PLUTO)

The PLUTO database ([City of New York, 2013](#)) is one of the most comprehensive land use datasets available through New York City's open data platform. It is distributed and regularly updated by the NYC Department of City Planning, and provides detailed information about

Table 1
Descriptive statistics of selected building characteristics from building footprint dataset.

	Mean	Std	Min	Max	Median
Height of roof [m]	8.28	6.13	0.00	429.27	7.91
Ground elevation [m]	16.69	12.59	-1.83	124.05	13.72
Area of footprint [m ²]	146.14	495.24	1.95	108,843.72	88.44
Number of floors	2.38	1.85	0.00	119.00	2.00

each tax lot (property) in the city including its address, zoning classification, lot area, and primary building characteristics. It is available in both tabular (as CSV files) and spatial format (as the "MapPLUTO" shapefile). In order to minimize the gap between LiDAR acquisition, we use PLUTO version 13v2 from October 2013. It describes 859,372 tax lots. Lot data from the PLUTO dataset can be joined with other administrative data sources using the BBL as a unique lot identification number. We use PLUTO data for the analysis of relationships between extracted building measures and other characteristics, such as gross floor area, proximity to other properties, and building age.

2.4. New York City 3-D building model

For validation purposes, we also use a NYC 3-D Building Model provided by the NYC Department of Information Technology & Telecommunications (DoITT). It is based on a 2014 aerial survey and planimetric database and contains all the buildings from that period, as defined by the NYC Building Footprint data (2.2). Individual 3-D building models were created by stereo compilation and photogrammetry in accordance to the CityGML standards. Models are based on a hybrid of the CityGML Level of Detail (LOD) 1 (prismatic buildings with flat roof detail) and LOD 2 (includes roof structure) ([Open Geospatial Consortium, 2012](#)). Approximately 100 iconic buildings were modeled to more detailed LOD 2.2 ([Biljecki, Ledoux, & Stoter, 2016](#)). In addition to the geometries, the data contain BIN information that can be used to map it to Building Footprint and PLUTO data. The data were provided in ESRI multipatch geodatabase file format allowing for surface and volume calculation with ESRI ArcGIS software.

3. Methods

The process for creating the DSM and extracting building parameters consists of multiple computational steps and associated data transformations. Our methodology is visually summarized in the flowchart ([Fig. 1](#)) and explained in detail below.

3.1. Creating the Digital Surface Model (DSM)

We begin by creating a Digital Surface Model (DSM) of New York City, which is a 3D representation of the terrain and surface of all objects from elevation data obtained from raw LiDAR point cloud data. This differs from a Digital Terrain Model (DTM), which represents ground surface only. We develop the DSM using LAStools and ESRI ArcGIS software ([ESRI, 2018; Isenburg, 2018](#)). The original LAS data were reprojected into the State Plane New York Long Island Zone 3104 geographical coordinate system using meters as both vertical and horizontal units. Unfortunately, the original LAS data provide return class information limited to ground, noise, and default, and built-in classifiers did not effectively distinguish buildings from vegetation in the complex and heterogeneous New York City landscape. Therefore, in order to remove major vegetation, we include single returns only for further processing. This reduces the volume of tree canopies as a single return is mostly associated with flat, solid surfaces - in the case of trees, the only remaining parts are trunks and major branches that in most cases do not grow above the building roof height. We also filter out any returns higher than 600 m, as the highest building in New York City is One World Trade Center with a reported height of 546.2 m ([CTBUH, 2018](#)). The entire study area was then encompassed by a rectangle bounding box, using the geographic extent of the most distant LiDAR data points, and divided into a 1 m grid. This approach minimized the impact of inconsistencies in the raw data and allowed for an immutable query time for each location, regardless of local point-cloud density. The result is a raster array with 46,877 columns and 47,361 rows, corresponding to real distance in meters. In order to obtain an estimated absolute height for each pixel, the maximum of filtered cloud points falling inside a given pixel is calculated. Nearest neighbor

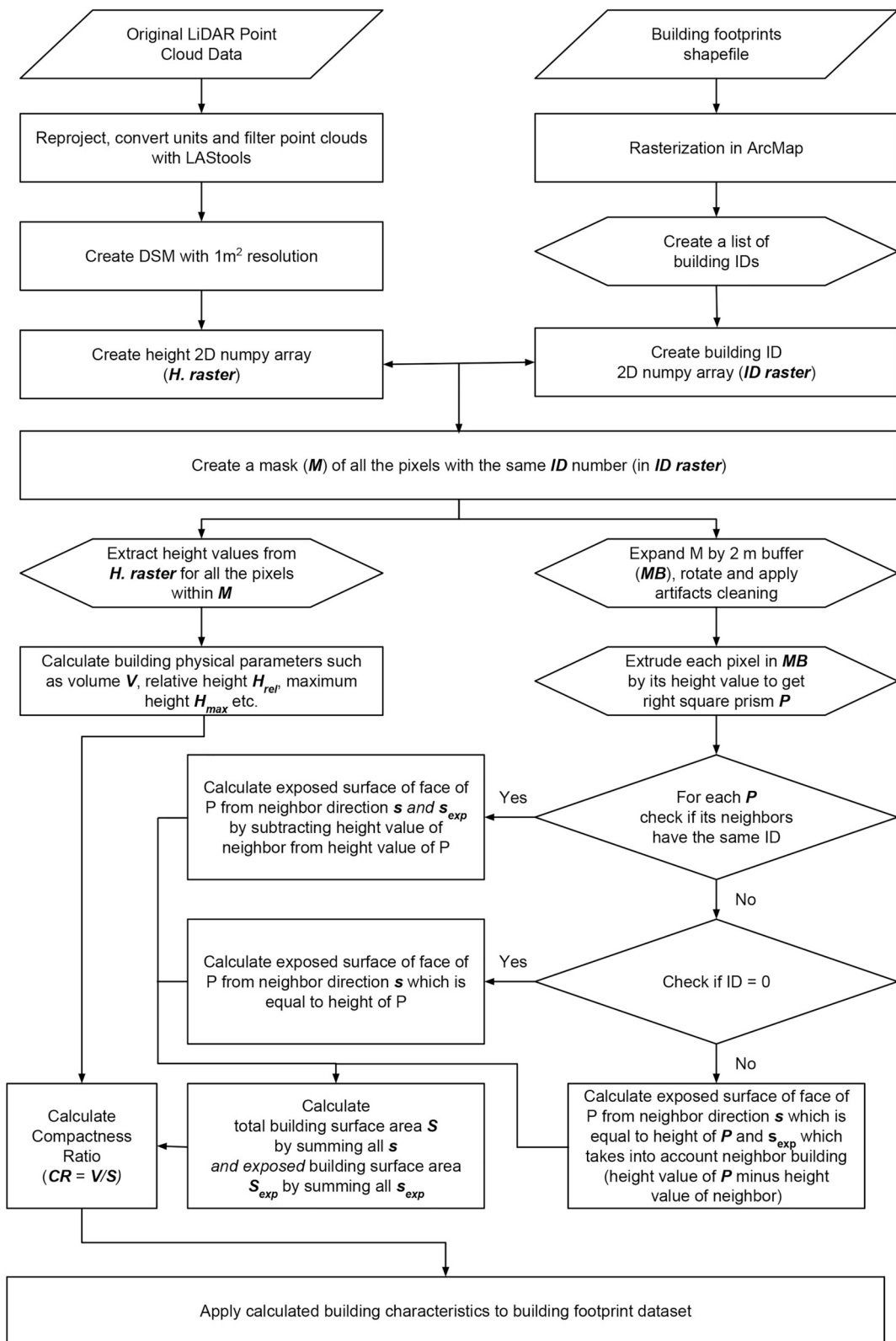


Fig. 1. Data processing flowchart.

interpolation is used to estimate the height of under-sampled pixels. The final output is a rasterized height-map of New York City - a DSM - where each pixel has specific geographic coordinates and represents 1 m² with associated maximum absolute height in meters. The DSM is visualized in Fig. 2.

3.2. Rasterizing building footprints

In order to match individual buildings with their height information, we create a two-dimensional array with building identification information of exactly the same size and geographical reference as the DSM. Building footprint data contains NYC-specific Building

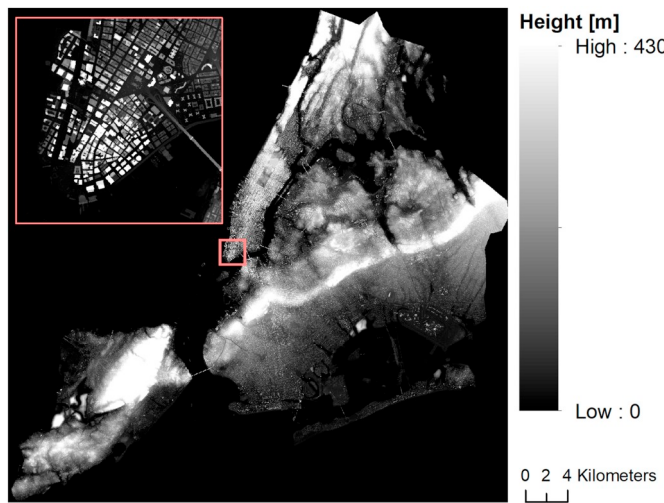


Fig. 2. Digital surface model of New York City.

Identification Numbers (BIN) assigned by the NYC Department of City Planning for each structure. However, this number is not unique as there are instances of duplications. Therefore, for each entry in the dataset we assign a unique ID in the form of integer from 0 to 1,082,433. Using the ESRI ArcMap software Feature to Raster tool, we create a raster where each 1 m^2 pixel represents the ID value of the building that covers a majority of the pixel area.

Both rasters (ID and DSM) are of the exact same size and geographic projection, as well as matched to the building footprint shapefile. This allows for querying and masking the DSM raster only for areas corresponding to the footprints of selected buildings based on their ID information. Fig. 3 shows part of Midtown Manhattan represented by both DSM (3a) and ID (3b) rasters. The brightness of the pixels indicate height in meters. One can easily notice that footprint-derived heights are homogeneous for the entire building area, while the DSM provides much greater variance in height information at much higher spatial resolution.

3.3. Extracting building models

The next step is to extract height values for each building in order to estimate the building's physical properties. Since both the ID and DSM rasters are aligned, we generate an algorithm to loop through every building ID, extract the location of all pixels with a given ID using the ID raster (Fig. 4b) and then mask the corresponding pixels in the DSM raster (Fig. 4a). The resulting two-dimensional pixel array contains height information only within a given property (Fig. 4c). The building model can then be reproduced by simple subtraction of the building

ground elevation (provided in the building footprint dataset) and extrusion of each pixel by its remaining height value (Fig. 4e). In order to estimate building exposed envelope surface area (S_{exp}), it is necessary to capture a building's surroundings, such as heights of adjacent buildings. For this reason, we expand the original mask by generating a 2 m exterior buffer around the identified building footprint (represented by the indigo outline in 4d). This captures adjacent property heights at points of contact between buildings (represented by green section).

In order to minimize the effect of building surface area overestimation due to voxelization, the algorithm aligns each property with the appropriate x and y axes. Considering the complexity of different building shapes, we set this alignment based on building edges rather than the building footprint outline. In most cases, it is rotated according to the outline, as these are the most pronounced structural edges. However there are multiple examples of buildings with rectangular footprint outlines, but much more complex structures, characterized with multiple set-backs and diamond or diagonal shapes. To allow this flexibility, we decide to use a combination of the Canny edge detection algorithm based on an array smoothed with $1 \times \sigma$ filter followed by a Progressive Probabilistic Hough Transform (PPHT) for straight line detection (Canny, 1986; Galamhos, Matas, & Kittler, 1999). The minimum length of the line was set as 10% of the length of the building array. The most common angle calculated for each of the detected lines is selected as a rotation angle for the entire array. Finally, artifacts from the array rotation operation are removed by flattening those pixels whose values differ by more than 50% from three out of four of their neighbors. The process is illustrated in Fig. 5.

3.4. Estimating building physical properties

The extraction of building height arrays allows for the estimation of multiple physical characteristics of the property, including building footprint area; maximum, minimum, median, and mean height; volume; envelope surface area; exposed envelope surface area; and compactness ratio. Equations for the calculation of these characteristics are presented in Table 2.

Measuring individual building volume is simplified by use of the 1 m DSM. Since each pixel has an area of 1 m^2 , the volume of the space above each pixel is equal to its height (in cubic meters). Therefore, the volume of each building is the sum of all its component pixels' height values - those contained within the defined building footprint perimeter extents - after subtracting the respective ground elevations.

To calculate the building envelope surface area, a *scanning plane* approach is used and is illustrated in Fig. 6. In order to capture the exposed envelope surface area (accounting for adjoining buildings that share walls), the expanded mask is used. Each building is treated as a voxelized object consisting of 1 m^3 cubes. Each pixel (P) masked by the building footprint is represented as a stack of voxels (volumetric pixels)

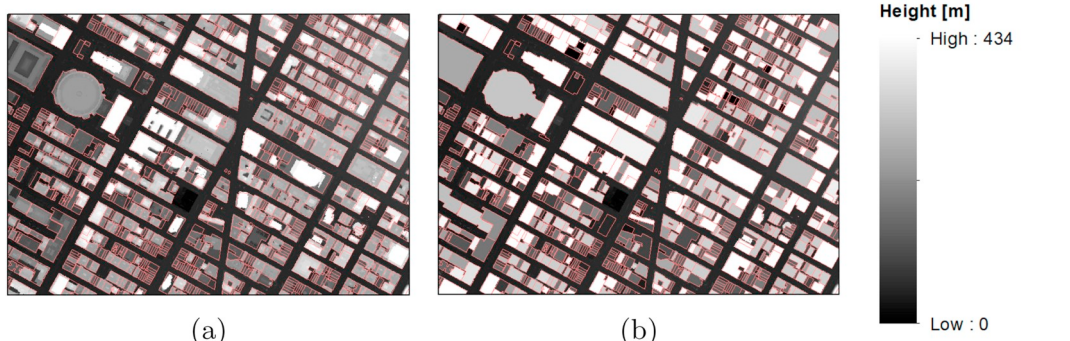


Fig. 3. Comparison of DSM (a) and rasterized building footprint (b) with overlayed building perimeters (red lines) of Midtown Manhattan. (For interpretation of the references to colour in this figure legend, the reader is referred to the web version of this article.)

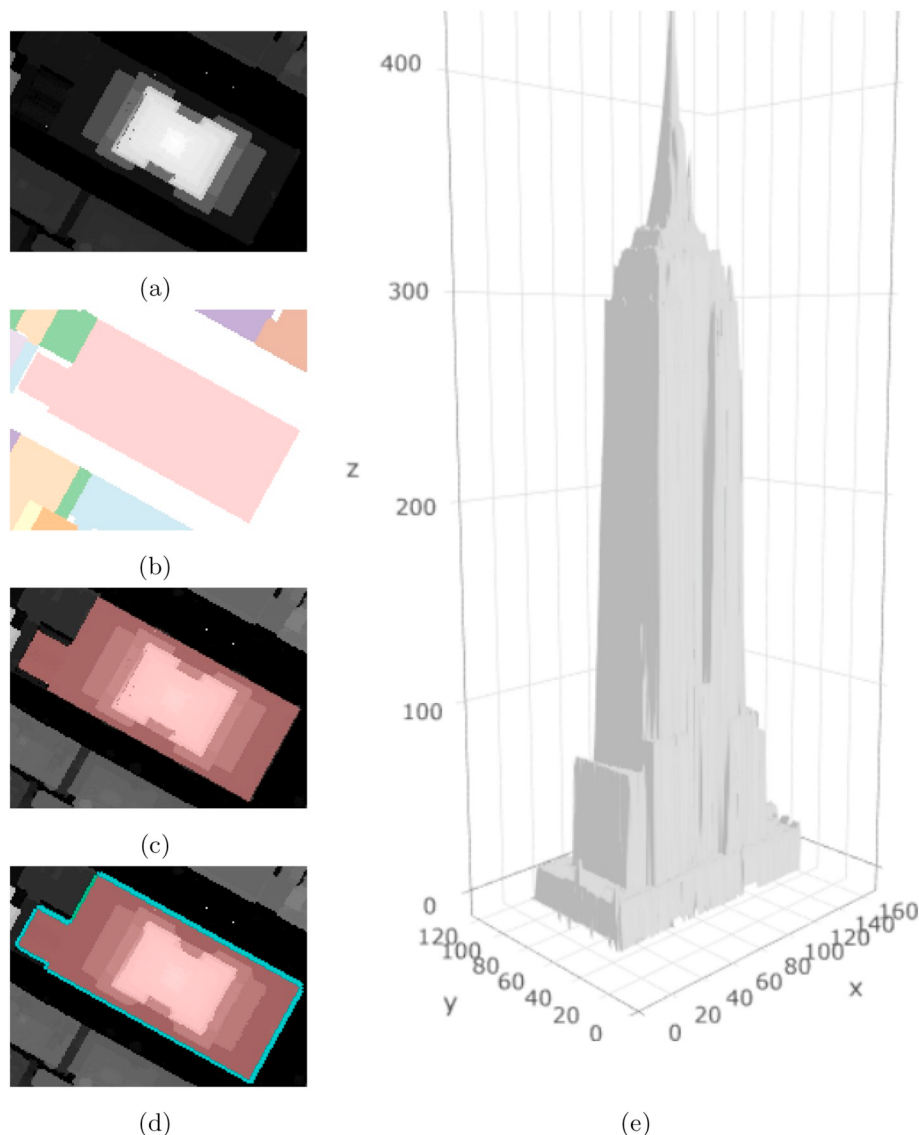


Fig. 4. DSM for Empire State Building (ESB) area (4a), identified ESB footprint area from building ID raster - pink (4b), extracted ESB heights from DSM (4c), 2 m buffer around ESB (indigo/green) allowing for surface area calculation (4d), ESB 3D model derived from DSM (4e). (For interpretation of the references to colour in this figure legend, the reader is referred to the web version of this article.)

(Laine, 2013; Nourian et al., 2016). The number of voxels (H_p) corresponds to the height equal to the DSM height value for pixel P subtracted by the ground elevation of the corresponding building. Summing all voxels in each stack generates a right square prism of 1 m base length and height of H_p with four (4) vertical faces with an area equal to $1 \times H_p$. The visible surface of each prism's face(s) is obtained by checking the height (H_p) of the neighboring pixel (P_b) and whether it

belongs to the same property (B). This test can have three potential results: (1) the neighboring pixel is assigned to the ground elevation, (2) it is assigned to the same building, or (3) it is assigned to an adjoining building. Each case impacts the calculation of the visible voxel's face surface or exposed face surface (s_{exp}). The procedure for each case is explained by Eqs. (1), (2) and (3):

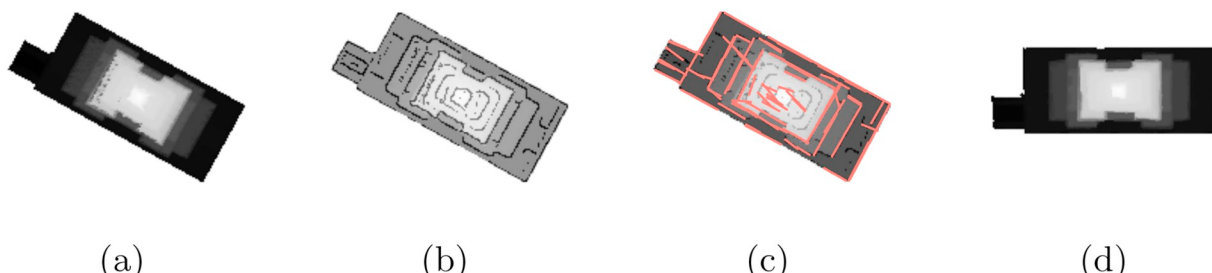


Fig. 5. Rotation processing for the ESB illustration; raw heights array (5a), superimposed edges detected with Canny algorithm (5b), superimposed straight lines identified with PPHT (5c), final ESB object after rotation and artifact removal (5d).

Table 2

Calculations for building physical properties.

Building property (units)	Calculation	
Ground area (m^2)	$A = N $	where: N is the set of pixels inside the building perimeter;
Maximum height (m)	$H_{\max} = \max(H) - H_0$	H is the set of height values of pixels inside the building perimeter; H_0 is the ground elevation of the property;
Volume (m^3)	$V = \sum_{i=1}^n H - (A \times H_0)$	
Envelope surface (m^2)	$S = \sum_{i=1}^n s + A$	s is the set of visible voxels' faces area;
Exposed envelope surface (m^2)	$S_{\exp} = \sum_{i=1}^n s_{\exp} + A$	s_{\exp} is the set of exposed visible voxels' face area
Compactness ratio (Exposed)	$CR = S \div V; (CR_{\exp} = S_{\exp} \div V)$	
Normalized compactness ratio (Exposed)	$nCR = \frac{CR}{((\sqrt[3]{V})^2 \times 5) \div V} = \frac{S}{(\sqrt[3]{V})^2 \times 5}; (nCR_{\exp} = \frac{CR_{\exp}}{((\sqrt[3]{V})^2 \times 5) \div V} = \frac{S_{\exp}}{(\sqrt[3]{V})^2 \times 5})$	

- P_b does not belong to any property:

$$s, s_{\exp} = H_p \quad (1)$$

- P_b belongs to the same property:

$$s, s_{\exp} = \begin{cases} H_p - H_p & \text{if } H_p > H_p \\ 0 & \text{if } H_p < H_p \end{cases} \quad (2)$$

- P_b belongs to different property:

$$s = H_p; \\ s_{\exp} = \begin{cases} H_p - H_p & \text{if } H_p > H_p \\ 0 & \text{if } H_p < H_p \end{cases} \quad (3)$$

The surface estimation algorithm ‘scans’ the voxelized building object, which is stored as a 3D array, using a vertical plane in two cardinal directions and calculates the sum of visible vertex face areas touched by the plane (Fig. 6). The total value is the estimated building surface area (S) (or S_{\exp} in the case of exposed building surface area) plus the horizontal surface area, which is equal to the building footprint area. The algorithm was implemented in Python using array functionality of the NumPy library (NumPy Developers, 2017; Python Software Foundation, 2017).

Estimating building volume and envelope surface area allows us to calculate individual building compactness ratios (CR), which is defined by the building's envelope surface area divided by its volume and also

known as the surface-area-to-volume ratio (Parasonis et al., 2012). It can be interpreted as a space efficiency metric describing how much space (in m^3) is enclosed by the building envelope area (in m^2). Since the CR scales with volume, for building-to-building comparisons it is necessary to normalize the calculated values. Theoretically, the maximum CR is achieved by a sphere. Since this form is not optimal for building form (given practical, architectural, and engineering constraints), the calculated CR is referenced to the CR of a cube of the same volume for a given building. The resulting normalized compactness ratio (nCR) allows for comparison between different buildings in the city.

4. Data quality

Despite the level of detail, data collection using LiDAR is not free from errors that can both affect rasterization and analysis. Also, rasterization itself introduces errors that need to be taken into account. We undertake several data cleaning steps in order to maximize data quality and reliability of the analysis.

4.1. LiDAR-related errors

Depending on the LiDAR technology used for generating point cloud data, it can be prone to inaccuracies in measurements, such as width of the laser ray or height, speed, and direction of the flyover. Accuracy depends greatly on the topography of the terrain (e.g. slopes can

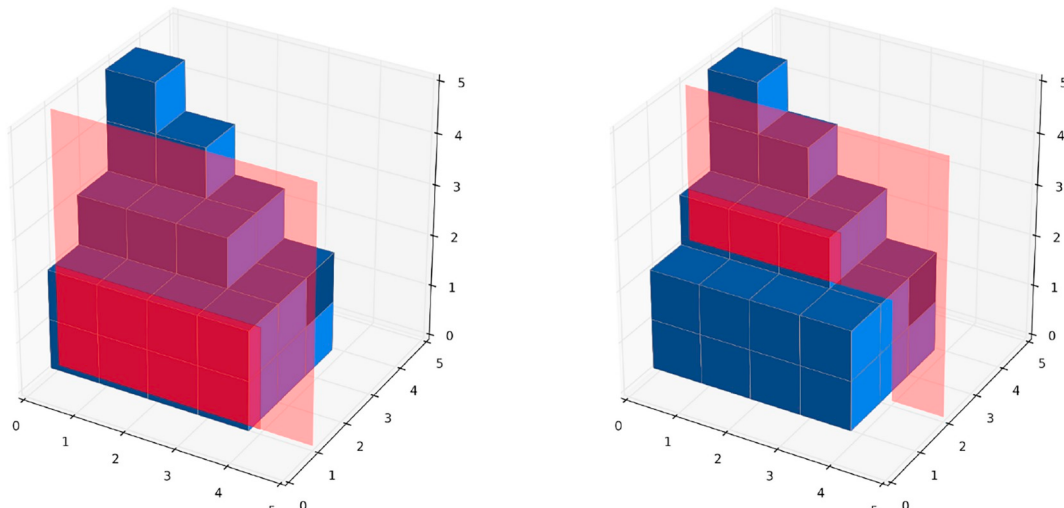


Fig. 6. Schematic illustration of envelope surface area calculation process. Blue voxels represent buildings, transparent red vertical plane loops through each pixel and sums all visible voxel faces. (For interpretation of the references to colour in this figure legend, the reader is referred to the web version of this article.)

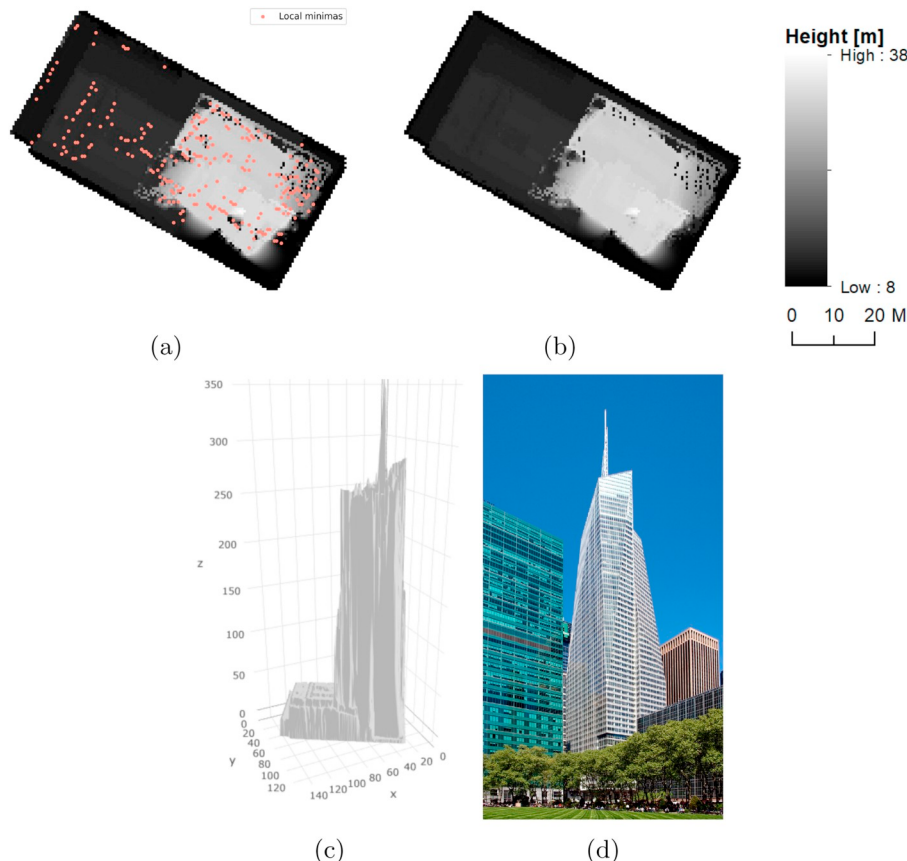


Fig. 7. One Bryant Park - example of a complex building form with multiple ‘crevasses’ in the DSM model: extracted DSM height model with identified local minimas (7a), cleaned DSM model (7b), 3D representation (7c) and actual building photograph (CTBUH, 2018) 7d.

introduce error into the reflected laser beam), its complexity (various and sudden setoffs, edges, and cliffs dissolve laser signals), as well as the type of the surface (plain, matte, and solid versus complex, highly reflective, and porous) (Jutzi & Stilla, 2003; Mallet & Bretar, 2009). It is especially true in the urban environment with an abundance of rapid changes in heights, surface materials, complexity of shapes, occlusions, etc. Errors in LiDAR measurements will affect the DSM and subsequent calculations of building physical properties.

In order to mitigate the impact of inaccurate data, we introduce several cleaning steps. Before creating the DSM, we remove outliers and filtered raw LiDAR data as described in section 3.1. When manipulating individual building models, we iteratively identify local minimas (‘crevasse’) using a 3 m² rolling window. This is in most cases enough to identify sudden drops in the DSM resulting from incorrect light beam reflection, while preserving edges and bigger structural concavities. When identified, a local minimum is replaced by the median value of the surrounding pixels, effectively filling the void in the building structure. This process is repeated until less than 100 local minimas are identified, which is arbitrarily chosen as an acceptable number. An example of an affected property is One Bryant Park (Fig. 7), where the angled glass facade and complex structure of the tower results in a fragmented DSM reproduction, while the lower portion of the building, which is more rectangular in shape, is more accurately depicted. It is visible especially in the north-eastern and south-western areas of the tower, where the laser beam penetrates through the glass surface inside the building (Fig. 7a).

4.2. Rasterization errors

Interpolation of the irregular raw point cloud LiDAR data onto the regular grid significantly reduces the size of the data and allows for

more efficient processing of larger, higher density urban areas, such as New York City. The cost of this efficiency are accuracy losses that introduce uncertainty into the model. Different interpolation methods have various effects on the final surface model, such as excessive smoothing or jagging of the resulting surface. Another consideration is the size of the grid. The rule of thumb is to use grid spacing similar, but not smaller than, the one of the original data (Smith, Holland, & Longley, 2004). In case of our New York City LiDAR dataset, point density is estimated to 2 points per m², therefore a grid cell size of 1 m² is appropriate. However, the character of the NYC landscape, defined by substantial height variations and a prevalence of vertical facade surfaces, results in a considerable number of underrepresented grid cells. To account for this, we fill in the missing values using mean values of the neighboring pixels.

The size of the grid cell also restricts the size of the detectable building footprint. In order to minimize systematic errors related to cell size, we validate the model estimated area of the building perimeter against values reported in the building footprint shapefile using Absolute Percentage Error (APE). In order to ensure data quality, we keep only those properties for which the APE is equal or smaller than 5%. In Fig. 8, one can observe that the relative error decreases with the size of property and follows roughly a power function of the form presented in the Eq. (4) where x equals the footprint area in m².

$$f(x) = 52.97 \times x^{-0.85} \quad (4)$$

Using this function, we establish a threshold for building footprint area of 15 m², for which the function estimated APE exceeds 5% (resulting in the exclusion of 7,975 properties) suggesting that the voxelization method becomes unreliable for the buildings with the smaller building footprint area. The resulting dataset still contains observations with significant discrepancies between reported and observed footprint

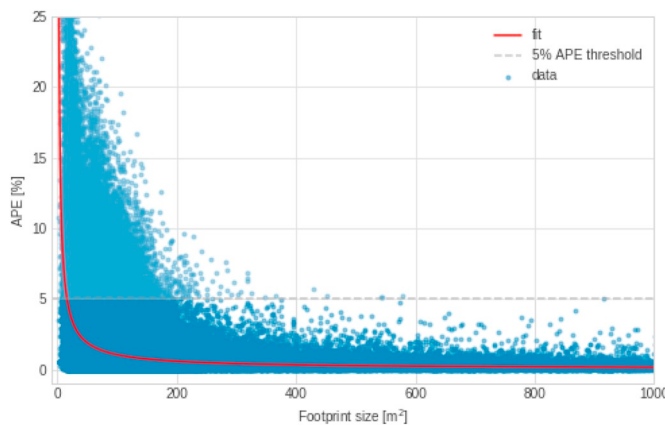


Fig. 8. Validation of LiDAR-based building footprint area (x-axis) vs. reported in building footprint data (y-axis). Red line represents fitted power function. (For interpretation of the references to colour in this figure legend, the reader is referred to the web version of this article.)

size; therefore, we additionally remove all of the observations with footprint area APE greater than 5%.

4.3. Data cleaning steps

Since the focus of this study is on building massing characteristics,

we remove properties with negative or missing volume and maximum height information. We also remove properties that were not constructed prior to the date of data acquisition (2013). From the original dataset of 1,082,433 properties, the following number of observations are dropped at each cleaning step:

- missing, negative or 0 volume - 1842 (0.2%)
- missing, negative or 0 height - 473 (0.04%)
- building footprint area smaller than 15 m^2 - 1283 (0.1%)
- building footprint area APE greater than 5% - 55,002 (5.1%)
- building constructed after 2013 - 728 (0.07%)

Fig. 9 shows the locations of removed properties. Many of the excluded smaller properties concentrate in the residential, lower density areas of the outer boroughs, especially in south Brooklyn and eastern parts of Queens, which can be associated with smaller structures, such as garages and sheds. The resultant clean dataset contains 1,070,147 buildings, which constitutes 98.9% of the total number of identified buildings in the study area.

5. Results and validation

Our algorithms estimate the physical parameters for buildings in New York City. Using a unique ID number, this information is integrated with building footprint data and assigned BBL and BIN identifiers that enable spatial joins with other city administrative data

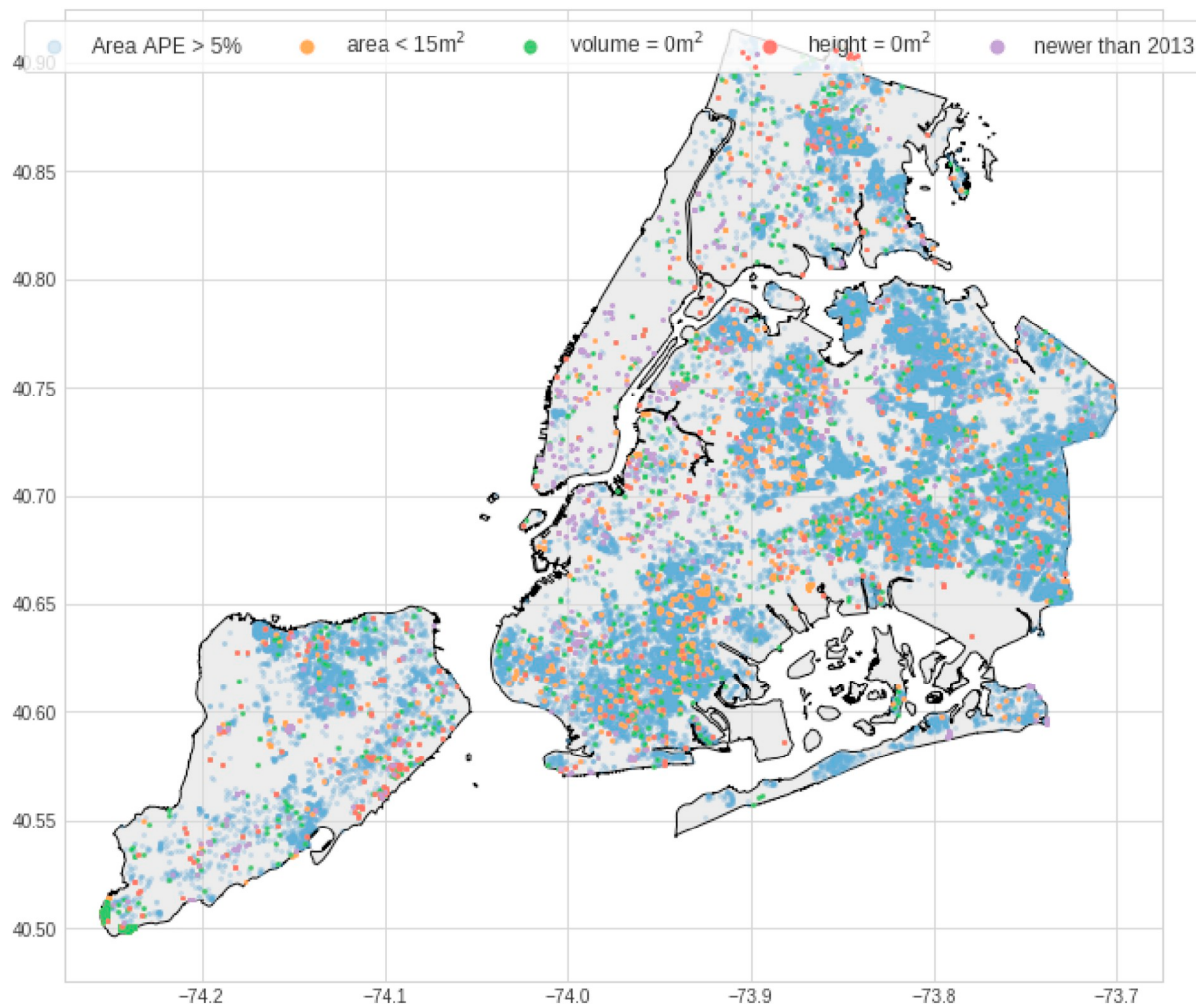
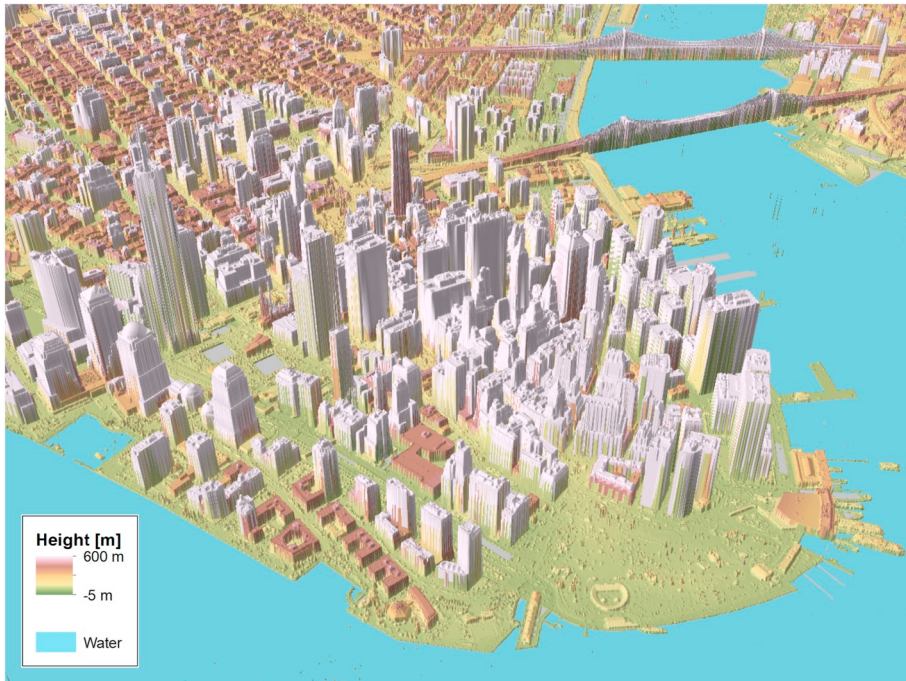


Fig. 9. Location of properties removed from the analysis.

Table 3

Descriptive statistics for selected building physical characteristics.

Metrics	Area [m ²]	Maximum height [m]	Volume [m ³]	Surface [m ²]	Exposed surface ratio	nCR
Mean	166.71	10.32	1853.15	710.64	0.56	1.19
Std	464.64	9.26	11,115.30	1703.52	0.15	0.17
Min	16.00	1.00	2.00	16.00	0.03	0.06
%	71.00	7.00	435.00	328.00	0.45	1.09
%	107.00	9.00	703.00	463.00	0.57	1.18
%	148.00	11.00	1056.00	619.00	0.68	1.27
Max	65,400.00	594.00	2,141,308.00	141,414.00	1.00	3.00

**Fig. 10.** 3D visualization of the volumetric model for the Lower Manhattan district of New York City, by calculated elevation.

records, such as land use, zoning, property tax, or energy consumption, among others. The script is written in the Python programming language and is executed on a large shared-memory machine with total memory of 1 TB and CPU Intel(R) Xeon(R) CPU E5-4640 0 @ 2.40GHz (4 × 8 cores). Over a period of 55 h, it processes more than 4.4 billion data points derived from the DSM raster and ID raster to create 1,082,433 voxelized building objects, extracts various measures, and saves results into CSV files and a dictionary of individual 2D building arrays. **Table 3** summarizes the descriptive statistics for selected metrics. The 3D visualization of our DSM-based volumetric model for the City is presented in **Fig. 10**. It shows the Lower Manhattan district of New York City colored by height.

Fig. 11 presents relationships between calculated features in the form of a scatterplot matrix. Not surprisingly, total surface area is closely correlated with building volume. Maximum height is correlated with both of these values, but without a similar strong relationship. As one can observe based on the distributions of each direct measurement, such as area, height, and volume (diagonal plots in the form of kernel density estimations), a majority of the properties are relatively small with a long tail of very large buildings. The distribution of exposed surface area values ranges from 0 to 1 and is characterized by three major peaks, suggesting three distinct building types, on which we elaborate further in **Section 5.2**.

5.1. Validation of basic metrics

Since there is no existing city-wide data repository with the ground-

truth values for our calculated building parameters, such as Building Information Models (BIM) or accessible architectural plans, validation of the model presents a challenge. For this reason, we use estimated values derived from aforementioned administrative datasets, namely the NYC Building Footprint and the NYC 3-D Building Model. Using CityGML standards ([Open Geospatial Consortium, 2012](#)) and more detailed classification proposed by [Biljecki et al. \(2016\)](#), we define them as LOD 1.2 and LOD 2.2 models, respectively. **Table 4** presents the relationship between the predicted (LiDAR-estimated) and observed (derived from administrative data) values for calculated physical characteristics together with estimated Median Percentage Error (MPE) for each.

DSM-based estimations for footprint area follow closely with CityGML values, with MPE near 0. Both volume and surface information is estimated relatively close to what is reported in both validation datasets with MPE values within 10%.

Another approach to validate building parameters results is to compare them to existing data for selected, well-documented properties. **Table 5** presents a summary of heights for selected, well-known tall buildings in New York City based on the official height data reported in the Global Tall Building Database of the Council on Tall Buildings and Urban Habitat (CTBUH) and our LiDAR-derived estimates. Similarly, to validate the volume results against ground truth information, we choose one of the best known buildings in New York City, which is the iconic Empire State Building. The volume of the ESB is reported to be 1,047,723 m³ ([Empire State Building, 2016](#)), while our model estimated 1,061,388 m³, which differs by only 1.3% from the reported

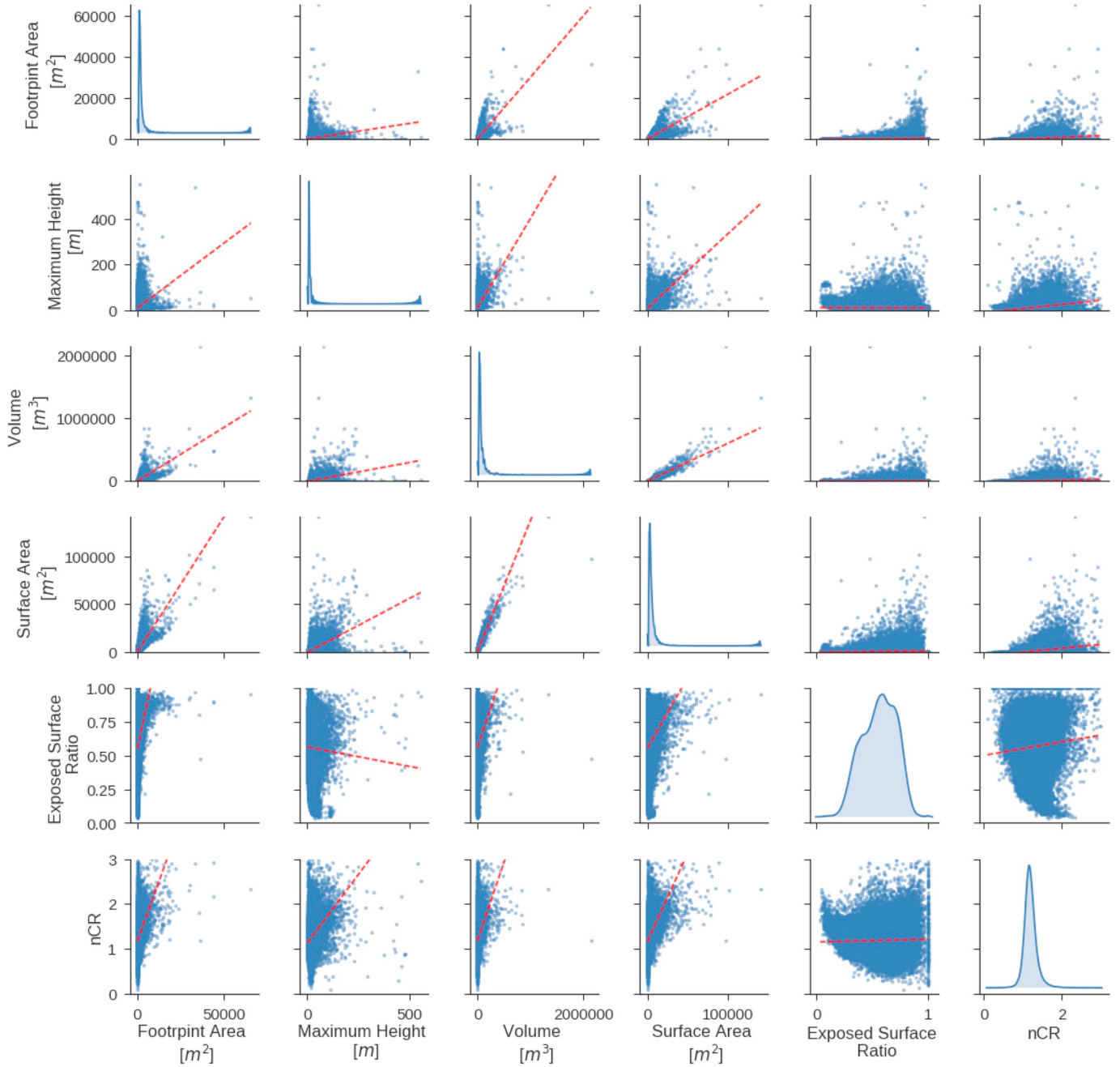


Fig. 11. Bivariate relationships between calculated physical characteristics of the buildings.

value. It is worth noting that our method captures the outside volume above the ground, while the report describes usable indoor volume.

5.2. Calculated metrics results - exposed Surface Ratio

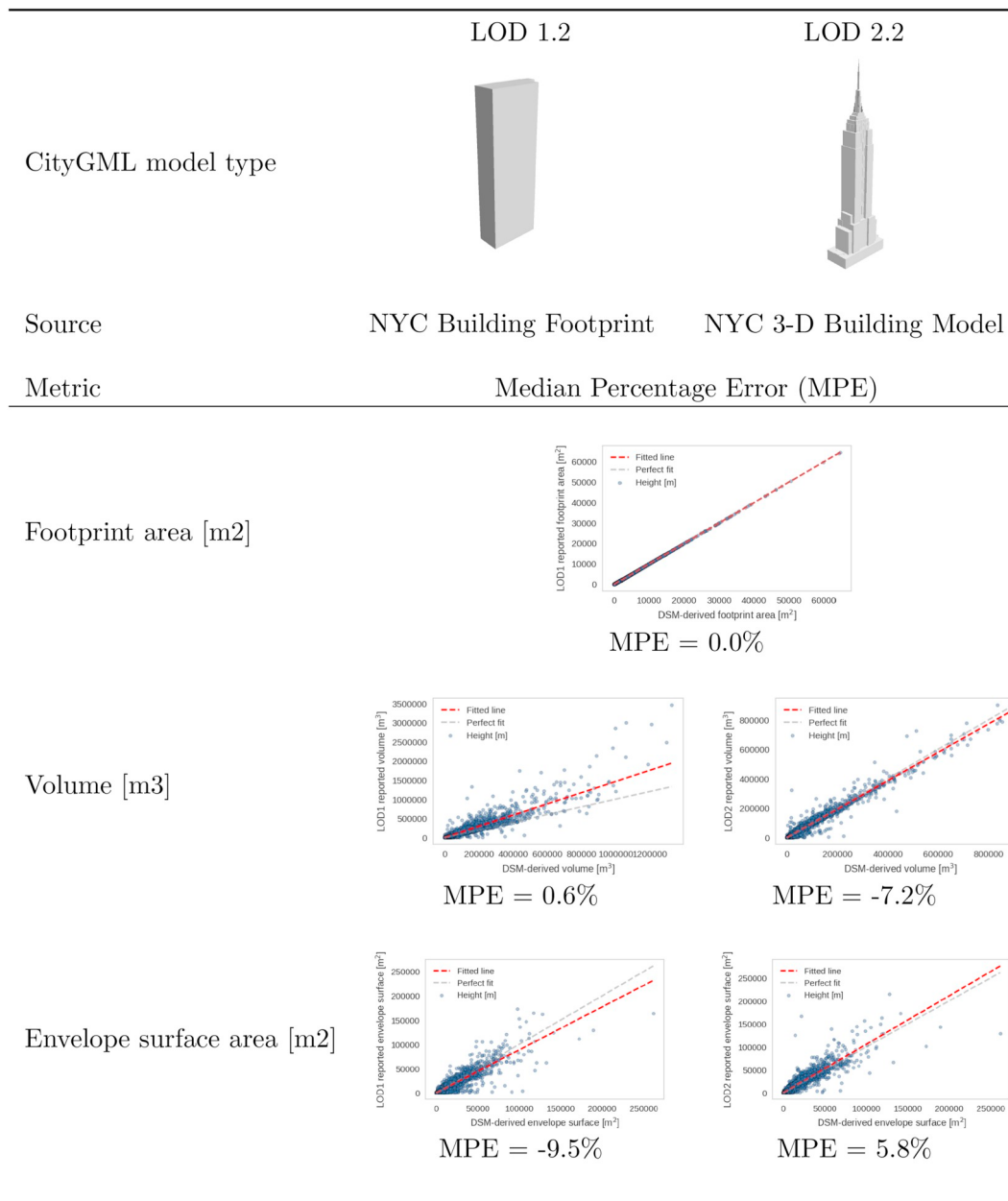
One important metric from a building performance perspective is the Exposed Surface Ratio (ESR), calculated as the ratio between the exposed surface area and total surface area of a building. Exposed surface area takes into account parts of the building envelope that are covered by or contiguous to other properties. An ESR equal to 1 means the building is a standalone (tower) property. Buildings adjacent to other buildings with shared (party) walls, will have lower ESR values since the exposed surface area is typically limited to the front and rear facades. Building adjacencies can be validated against the PLUTO dataset, which includes a “Proximity Code” variable for each lot that distinguishes between *detached*, *semi-attached*, and *attached* lot types

based on the spatial relationship to neighboring properties. The boxplot in Fig. 12a shows the distribution of ESR values for each proximity code category. Detached buildings have the highest ESR values of approximately 0.7, while semi-attached and attached buildings have ratios around or below 0.5, depending on the extent of shared vertical surfaces.

After merging our calculated building characteristics with the building footprint and PLUTO datasets, we analyze the relationship between ESR and other building features, such as age and gross floor area. The ESR distribution for buildings of different ages (by decade built) is presented in Fig. 12b. It can be observed that median ESR values were increasing until the 1920s and stabilized above 0.6 until the 1970s, and then fell again, maintaining an average level of 0.5 until the present. One reason for this is the decreasing availability of land, requiring infill development on smaller lots, particularly in areas with access to transit infrastructure. Analyzing the distributions of ESR

Table 4

Results validation against LOD 1.2 and LOD 2.2 datasets.

**Table 5**

Comparison of official building heights and LiDAR-derived estimation in meters.

Building	CTBUH [m]	LiDAR-based [m]
One World Trade Center	546	543
Empire state building	443	440
Bank of America Tower	366	367
Chrysler Building	319	289
New York Times Tower	319	317

against the total floor area of each building (Fig. 12c) shows that very small (below 50 m²) and very large properties (above 50,000 m²) tend to have higher median ESR values (0.7), followed by mid-sized buildings (between 1000 and 25,000 m²). This finding validates our approach, as the smallest properties are predominantly stand-alone single-family homes (such as those in low-density areas of Staten Island and

Queens), while the largest properties are characterized by high-rise towers with substantial exposed surface planes. Properties with the lowest median ESR value are those between 250 and 1000 m², which are typically one- or two-family, multi-family, or mixed use walk-up buildings, like the iconic “brownstones” of Brooklyn.

ESR can be used as a new metric to describe urban morphology and density by indicating how closely buildings are situated in relation to each other (indicative of a prevalence of stand-alone properties vs. infill, higher-density development, for instance). Fig. 12d shows the distribution of ESR values for each NYC borough. Queens (QN) and Staten Island (SI) have the majority of free-standing properties in the City with the highest median ESR values around 0.6. Manhattan (MN), on the other hand, is characterized by dense, compact development, evidenced by the lowest median ESR below 0.5.

The map in Fig. 13 provides more detailed information on the spatial distribution of ESR values across the City. It supports previous findings about Queens and Staten Island, where large areas are shown

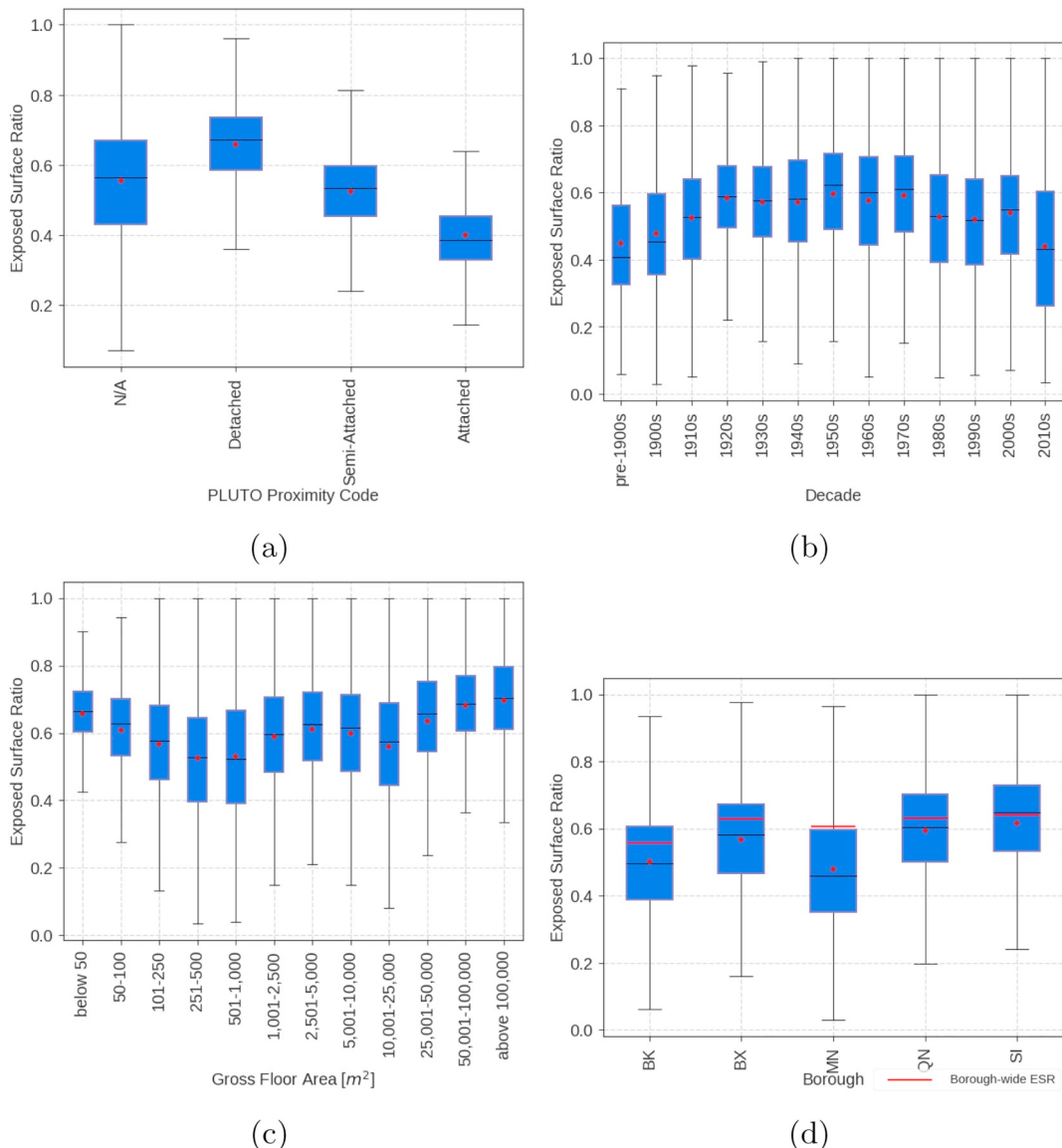


Fig. 12. Box-and-whisker plots of Exposed Surface Ratios by PLUTO proximity type (12a), decade built (12b), total gross floor area (12c) and Borough (12d) (red dot is a mean value). (For interpretation of the references to colour in this figure legend, the reader is referred to the web version of this article.)

in dark blue indicating higher ESR values. On the other hand, a majority of Manhattan (particularly the entire area South of 110th Street and parts of Harlem), as well as the Northern parts of Brooklyn, are found to have lower ESR values, given the nature of development in these areas. This metric provides a measure of urban density at high resolution, and introduces an alternative method to typical approaches such as floor area per land area or number of residential units per areal unit.

5.3. Calculated metrics results - compactness Ratio

As stated previously, building compactness is another critical metric in the analysis of building form, from both design and performance perspectives (Ourghi et al., 2007; Parasonis et al., 2012). The calculated normalized compactness ratios (nCR) for NYC buildings ranges from 0.54 to 1.90 (after removing the top and bottom 1% of calculated values as outliers) with a mean value of 1.19. Lower values indicate a more compact and efficient building form, maximizing volume and minimizing total envelope surface area. Fig. 14 provides a visual comparison of examples of low (42–30 Union Street in Queens) and high compactness (221 Kingston Avenue in Brooklyn) buildings. They

both share similar characteristics, such as footprint size (676 and 678 m^2) and gross floor area (3334 and 3287 m^2); however, their compactness ratios are 1.68 and 1.22, respectively. Looking at their shapes, it is clearly visible that the envelope surface area of the building in Fig. 14a is almost doubled due to a deep yard in the central part of the building and long, relatively narrow wings. On the other hand, the latter building has a base shape very similar to a cube with a domed roof. Compactness of the sphere exceeds that of a cube, therefore this building's nCR value is significantly lower.

Similar to ESR values, nCRs vary with building age, size, and location (Fig. 15), which is representative of the architectural styles and zoning regulations at different periods of time and across different parts of the City.

Fig. 15a shows changes in nCR based on building age. One can observe consistent level of the mean nCR values until the end of the 1930s around 1.2, and then a slight drop to around 1.15 since then with the lowest values in the 60 s. There might be several factors explaining this, one of which is the introduction of a new zoning code in 1961 requiring buildings to comply with specific floor-area ratio (FAR) requirements, as well as the introduction of new construction and curtain-wall technologies. Sudden increase in the 2010s can be attributed to

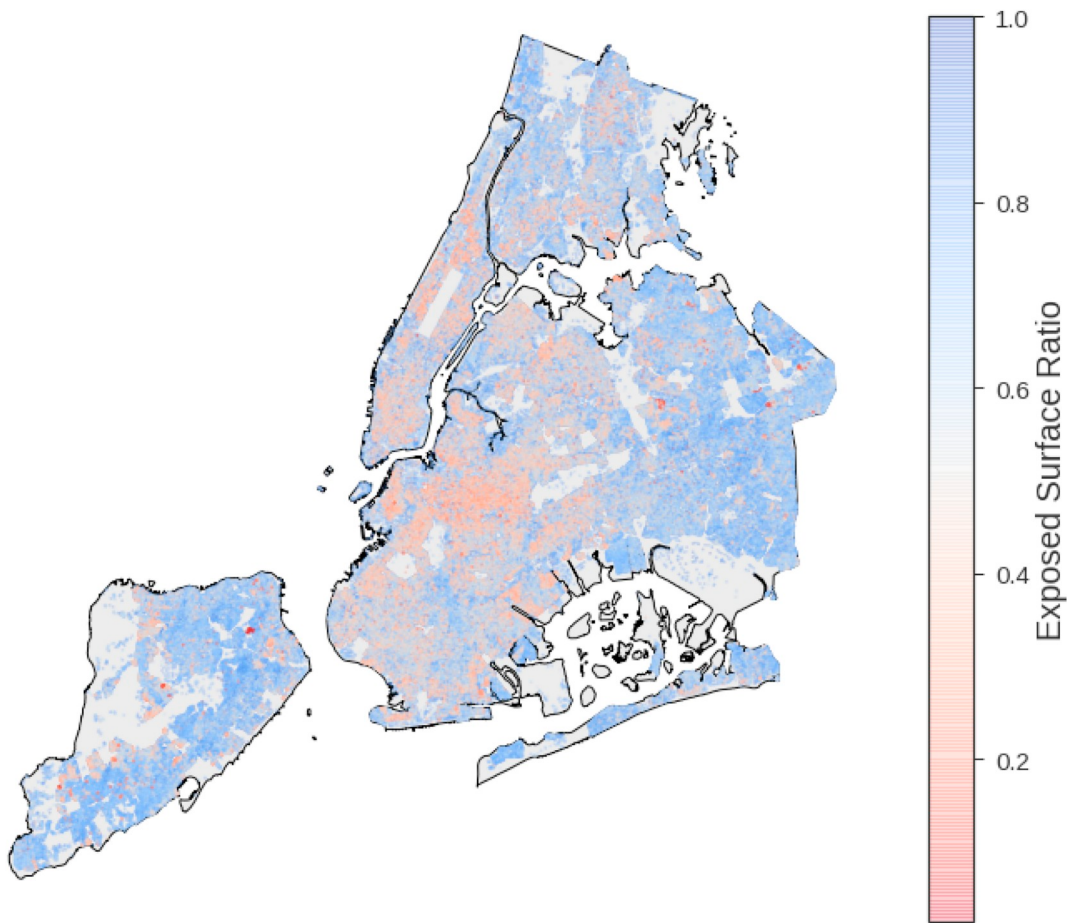


Fig. 13. Map of spatial distribution of exposed surface ratio of NYC properties.

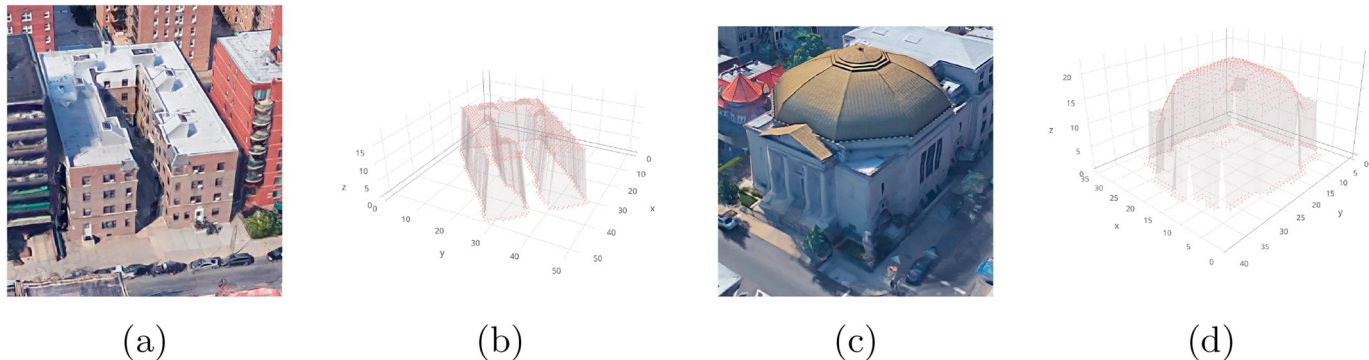


Fig. 14. Examples of high nCR building (42–30 Union Street, Queens, NY - Google Earth view: 14a, DSM 3D model: 14b) and low nCR building (221 Kingston Avenue, Brooklyn, NY - Google Earth view: 14c, DSM 3D model: 14d).

very small sample size.

The relation between nCR and total building floor area (Fig. 15b) shows a slight positive correlation as mean nCR values increase with building size. This may be caused by lot size restrictions and specific zoning requirements. The largest buildings in the City are constrained by relatively small lot sizes, which leads to vertical expansion for additional square footage. As a result, buildings take much narrower and taller shapes, typically with setbacks as the height increases. Interestingly, there is higher dispersion in the distribution of nCR values for larger properties compared to smaller buildings, indicating greater variability in design for large properties, even though they are less numerous (88% of the building stock are less than 500 m²).

Analysis of nCR values by borough (Fig. 15c) shows that less dense

areas of outer boroughs tend to have lower mean compactness ratios around 1.2. The highest observed mean nCR value is in Manhattan ranging from 1.2 to 1.5. This is again a function of lot size and higher land value, pushing developers to build on as much of the available lot area as possible. Since a typical lot size has a form of a rectangle with dimensions of 25 × 100 ft or 50 × 100 ft (which is 7.62 × 30.48 m or 15.24 × 30.48 m), buildings tend to be narrow, long and relatively tall, while courtyards and air shafts significantly reduce measured compactness.

The compactness ratios of individual buildings (map in Fig. 16) support the general, borough-wide trend. The entire Borough of Manhattan is populated by buildings of higher compactness, specifically in Downtown and Midtown Manhattan and residential areas of Upper East

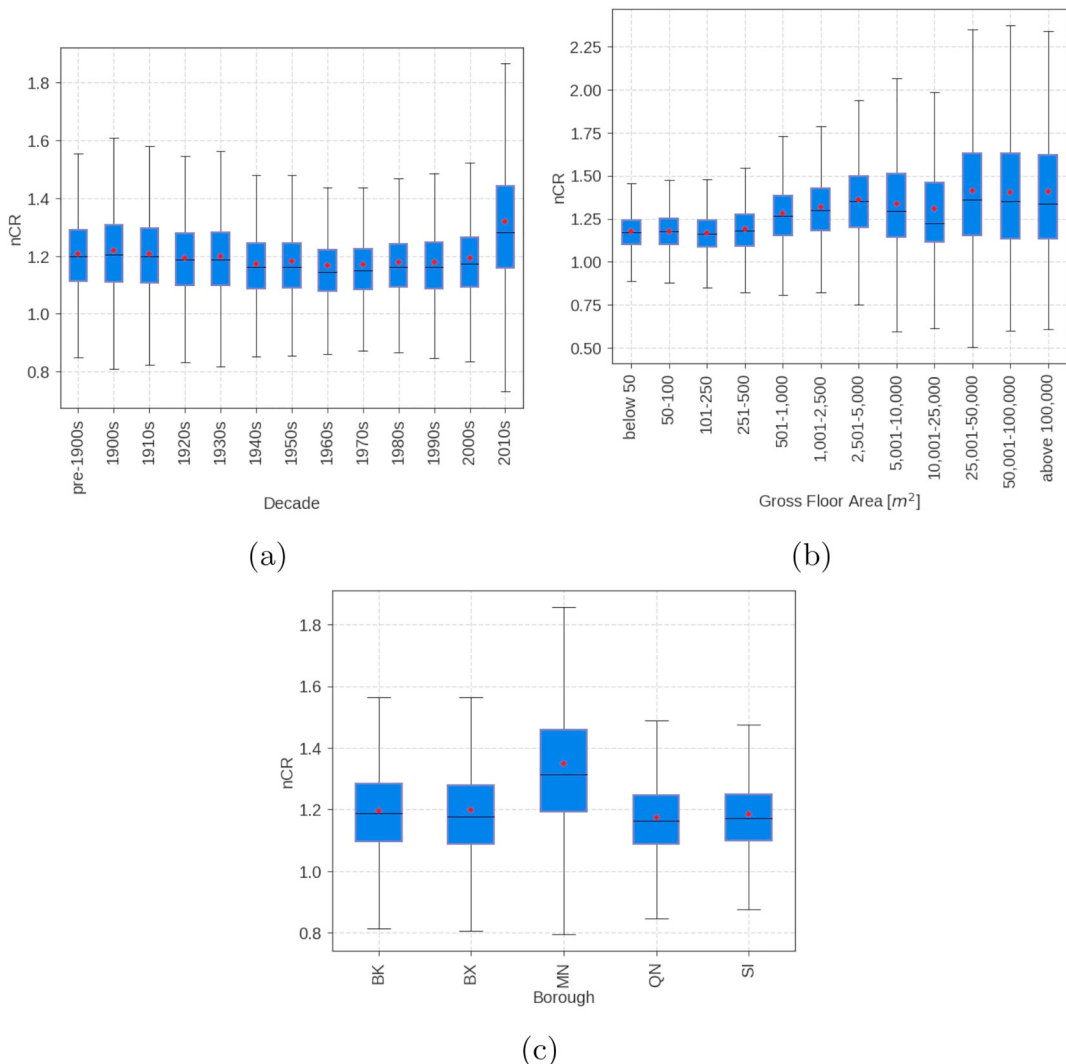


Fig. 15. Box-and-whisker plots of compactness ratios by decade built 15a, total gross floor area 15b and by borough 15c (red dot is a mean value). (For interpretation of the references to colour in this figure legend, the reader is referred to the web version of this article.)

Side, Upper West Side and Washington Heights to the north. Areas further from the city center, like Staten Island, eastern parts of Queens, the Bronx, and south Brooklyn, are less densely populated and characterized by single family homes with lower compactness ratios.

6. Discussion and limitations

The described methodology uses voxelization to generate individual building models and building form metrics, including height, volume, envelope surface, and compactness ratio, which together provide a detailed volumetric and morphological representation of the city from LiDAR-derived DSM. The results can be used as a valuable source of information for several applications within the urban domain. These include the evaluation of building performance based on design and form (such as the case of energy efficiency, for example) and the analysis of building massing and density for urban planning and zoning purposes, including shadow analysis, solar access, or air pollution or particulate dispersion. Integrating DSMs from multiple years allows for detailed tracking of city development and associated morphological changes at the building, neighborhood, and city scales. Unlike CityGML modeling, DSM generation is a generalizable process using LiDAR point cloud data, and therefore can be easily replicated whenever new LiDAR data are available.

Our methodology has several limitations. ALS-based LiDAR is can be

prone to occlusion effects, which means it will not capture information about overhangs, awnings, and tunnels at scale. Also, DSM quality is closely related to the accuracy and quality of the LiDAR point cloud itself. Low point cloud density, lack of intensity information, or limited point classification can hinder complete DSM processing, such as removing vegetation or improperly reflected laser beams. Furthermore, the process of rasterization can introduce uncertainty into the model, although this is balanced against the computational efficiency benefits in terms of data size and processing.

The proposed workflow relies on auxiliary data, namely building footprints, to locate individual buildings and merge with other administrative datasets. However, with LiDAR point cloud data, it is possible to extract this information, as well as ground elevation, as an additional pre-processing step. Relying solely on a DSM, though, can make this process significantly more complex and less reliable. To address this concern, there is a growing number of institutions providing building footprint information, such as local administrative repositories or crowd-sourced mapping services (e.g. OpenStreetMap) that can be used to replicate our method in other urban areas.

7. Conclusion

Our city-scale building morphology extraction method creates a high resolution model of city and building topography that can

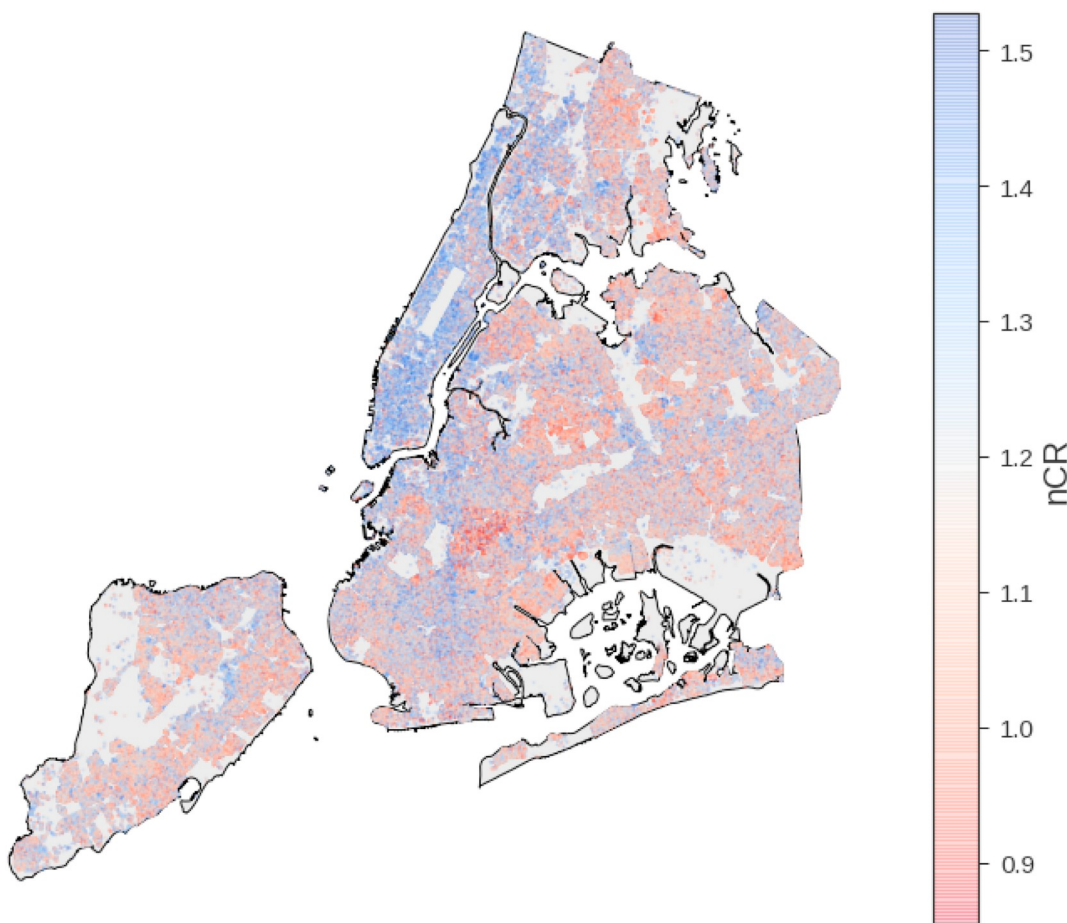


Fig. 16. Map of spatial distribution of compactness rates of NYC properties.

calculate otherwise unavailable or difficult to collect building parameters in a computationally-efficient manner. In particular, the calculation of exposed surface area and normalized compactness ratio metrics provide new ways to assess the density, footprint, and overall design efficiency of the built environment. Therefore, the approach represents significant potential value for city administrators, urban planners, architects, building designers and researchers to better understand the effects of urban morphology on a range of quality-of-life issues. This work can support evidence-based and data-driven studies into persistent questions of how the form of a city and its buildings influence critical long-term challenges of sustainability, resilience, and human well-being.

Our methodology can be readily scaled to other cities beyond the New York City example used here. For instance, the Taiwanese government has made a substantial investment in LiDAR through the Taiwanese LiDAR Project. Similarly efforts are underway in cities such as Vancouver, Canada and Philadelphia, Pennsylvania. The rapidly decreasing cost of acquiring aerial LiDAR data together with increasing accuracy will further expand the number of urban areas with available morphological data. Given the complexity of these, and many other, urban environments, our large-scale demonstration of the viability of our method in New York City can have far-reaching applications. Depending on available datasets, our approach can provide important insights and contribute to a more complete understanding of building dynamics, the effect of the urban heat island, wind dynamics of ‘urban canyons’, and many other questions of urban physics.

Acknowledgments

The authors would like to thank the New York City Mayor's Office of

Sustainability and the Department of Information Technology and Telecommunications for access to the relevant datasets. This material is based upon work supported, in part, by the National Science Foundation under Grant No. 1653772. All errors remain our own.

References

- Ahearn, S. C., & Ahn, H. J. (2011). Quality assurance and potential applications of high density lidar data for the city of new york. *Proceedings American society of photogrammetry and remote sensing* (Milwaukee Wisconsin).
- Alhaddad, B. I., Roca, J., Burns, M. C., & Garcia, J. (2008). Satellite imagery and lidar data for efficiently describing structures and densities in residential urban land uses classification. *ISPRS - International Archives of the Photogrammetry, Remote Sensing and Spatial Information Sciences*. <https://doi.org/10.5194/isprsarchives-XL-4-W1-71-2013> Accessed May 2016.
- Biljecki, F., Ledoux, H., & Stoter, J. (2016). An improved lod specification for 3d building models. *Computers, Environment and Urban Systems*, 59, 25–37. <http://www.sciencedirect.com/science/article/pii/S0198971516300436>. <https://doi.org/10.1016/j.compenvurbsys.2016.04.005>.
- Canny, J. (1986). A computational approach to edge detection. *IEEE Transactions on Pattern Analysis and Machine Intelligence, PAMI-8*, 679–698. <https://doi.org/10.1109/TPAMI.1986.4767851>.
- Carneiro, C., Morello, E., Ratti, C., & Golay, F. (2009). Solar radiation over the urban texture: Lidar data and image processing techniques for environmental analysis at city scale. In J. Lee, & S. Zlatanova (Eds.). *3D Geo-information sciences* (pp. 319–340). Berlin: Springer Berlin Heidelberg Chapter 20.
- Center for Advanced Research of Spatial Information - CARSI. *The New York city solar map*. (2016). <http://nycsolarmap.com/> (Accessed May 2016).
- City of New York (2013). Pluto 13v2. [https://www1.nyc.gov/site/planning/data-maps/open-data/bytes-archive.page?sorts\[year\]=0](https://www1.nyc.gov/site/planning/data-maps/open-data/bytes-archive.page?sorts[year]=0), Accessed date: May 2018.
- City of New York (2015). Building footprints. <http://www1.nyc.gov/site/planning/data-maps/open-data.page>, Accessed date: May 2016.
- City of New York (2017). Nyc Planimetric database. https://github.com/CityOfNewYork/nyc-planimetrics/blob/master/Capture_Rules.md, Accessed date: May 2017.
- CTBUH (2018). Skyscraper center. <http://www.skyscrapercenter.com>, Accessed date: June 2018.
- Depecker, P., Menezo, C., Virgone, J., & Lepers, S. (2001). Design of buildings shape and

- energetic consumption. *Building and Environment*, 36(5), 627–635.
- Dias, J. M. S., Bastos, R., Correia, J., & Vicente, R. (2006). Semiautomatic 3d reconstruction of urban areas using epipolar geometry and template matching. *Computer-Aided Civil and Infrastructure Engineering*, 21, 466–485. <https://doi.org/10.1111/j.1467-8667.2006.00452.x>.
- Empire State Building (2016). Empire state building fact sheet. http://www.esbnyc.com/sites/default/files/esb_fact_sheet_4.9_14.4.pdf, Accessed date: May 2016.
- ESRI (2018). Arcgis desktop: Release 10.6. <http://rapidlasso.com/LAStools>, Accessed date: March 2018.
- Galamhos, C., Matas, J., & Kittler, J. (1999). Progressive probabilistic hough transform for line detection. *Proceedings. 1999 IEEE computer society conference on computer vision and pattern recognition (Cat. No PR00149)*. Vol. 1. *Proceedings. 1999 IEEE computer society conference on computer vision and pattern recognition (Cat. No PR00149)* (pp. 560–). . <https://doi.org/10.1109/CVPR.1999.786993>.
- Glaeser, E. (2011). *Triumph of the city: How our greatest invention makes us richer, smarter, greener, healthier, and happier*. Penguin Publishing Group<https://books.google.com/books?id=yWTIKsWGM4c>.
- Gonzalez-Aguilera, D., Crespo-Matellan, E., Hernandez-Lopez, D., & Rodriguez-Gonzalvez, P. (2013). Automated urban analysis based on lidar-derived building models. *IEEE Transactions on Geoscience and Remote Sensing*, 51, 1844–1851. <https://doi.org/10.1109/TGRS.2012.2205931>.
- Goodwin, N. R., Coops, N. C., Tooke, T. R., Christen, A., & Voogt, J. A. (2009). Characterizing urban surface cover and structure with airborne lidar technology. *Canadian Journal of Remote Sensing*, 35, 297–309. <https://doi.org/10.5589/m09-015>.
- Google (2017). Google Earth View of New York City. <https://https://www.google.com/maps/@40.7109624,-74.011574,547a,35y,353.52h,29.22t/data=!3m1!1e3>, Accessed date: June 2017.
- Grindgis.com (2015). LiDAR data 50 applications and uses- it is important. <http://grindgis.com/data/lidar-data-50-applications>, Accessed date: May 2016.
- Haarap, R., & Lato, M. (2016). An overview of LiDAR for urban applications. http://geol.queensu.ca/faculty/harrap/pdf/WhatIsLiDAR_release1.pdf.
- Iserburg, M.. Lastools - efficient lidar processing software. (2018). <http://rapidlasso.com/LAStools> (Accessed March 2018).
- Jutzi, B., & Stilla, U. (2003). Laser pulse analysis for reconstruction and classification of urban objects. *The International Archives of the Photogrammetry, Remote Sensing and Spatial Information Sciences*, 34, 151–156.
- Kontokosta, C. E. (2015). A market-specific methodology for a commercial building energy performance index. *The Journal of Real Estate Finance and Economics*, 51, 288–316. <https://doi.org/10.1007/s11146-014-9481-0>.
- Kontokosta, C. E., & Tull, C. (2017). A data-driven predictive model of city-scale energy use in buildings. *Applied Energy*, 197, 303–317. <http://www.sciencedirect.com/science/article/pii/S0306261917303835>. <https://doi.org/10.1016/j.apenergy.2017.04.005>.
- Laine, S. (2013). A topological approach to voxelization. *Computer Graphics Forum*, 32, 77–86. <https://onlinelibrary.wiley.com/doi/abs/10.1111/cgf.12153>. <https://doi.org/10.1111/cgf.12153>.
- Lwin, K. K., & Murayama, Y. (2011). Estimation of building population from lidar derived digital volume model. In Y. Murayama, & R. B. Thapa (Eds.). *Spatial analysis and modeling in geographical transformation process* (pp. 87–98). Netherlands: Springer Chapter 6.
- Mallet, C., & Bretar, F. (2009). Full-waveform topographic lidar: State-of-the-art. *ISPRS Journal of Photogrammetry and Remote Sensing*, 64, 1–16. <http://www.sciencedirect.com/science/article/pii/S0924271608000993>. <https://doi.org/10.1016/j.isprsjprs.2008.09.007>.
- Matel, B. C., Sawhney, H. S., Samarasekera, S., Kim, J., & Kumar, R. (2008). Building segmentation for densely built urban regions using aerial lidar data. *Computer Vision and Pattern Recognition, 2008. CVPR 2008. IEEE Conference* (pp. 1–8). . <https://doi.org/10.1109/CVPR.2008.4587458>.
- Neidhart, H., & Brenner, C. (2003). Automatic calculation of building volumes for an area-wide determination of heat requirements. In P. I. C. I. J. Workshop (Ed.). *Challenges in Geospatial Analysis, Integration and Visualization II*.
- Nourian, P., Gonçalves, R., Zlatanova, S., Ohori, K. A., & Vo, A. V. (2016). Voxelization algorithms for geospatial applications: Computational methods for voxelating spatial datasets of 3d city models containing 3d surface, curve and point data models. *MethodsX*, 3, 69–86.
- NumPy Developers (2017). Numpy - package for scientific computing with python. <http://www.numpy.org/>, Accessed date: March 2017.
- Open Geospatial Consortium (2012). *OGC CITY Geography Markup Language (CityGML) encoding standard*. Technical Report Open Geospatial Consortium, Accessed date: August 2018.
- Open Geospatial Consortium (2018). CityGML. <http://www.opengeospatial.org/standards/citygml>.
- OpenStreetMap contributors (2018). Planet dump. retrieved from <https://planet.osm.orgh><https://www.openstreetmap.org>.
- Ourghi, R., Al-Anzi, A., & Krarti, M. (2007). A simplified analysis method to predict the impact of shape on annual energy use for office buildings. *Energy Conversion and Management*, 48, 300–305. <http://www.sciencedirect.com/science/article/pii/S096890406001397>. <https://doi.org/10.1016/j.enconman.2006.04.011>.
- Pacheco, R., Ordez, J., & Martnez, G. (2012). Energy efficient design of building: A review. *Renewable and Sustainable Energy Reviews*, 16, 3559–3573. <http://www.sciencedirect.com/science/article/pii/S1364032112002286>. <https://doi.org/10.1016/j.rser.2012.03.045>.
- Parasonis, J., Kezikas, A., & Kalabatiene, D. (2012). The relationship between the shape of a building and its energy performance. *Architectural Engineering and Design Management*, 8, 246–256. <https://doi.org/10.1080/17452007.2012.675139>.
- Poullis, C., & You, S. (2009). Automatic reconstruction of cities from remote sensor data. *Computer Vision and Pattern Recognition, 2009. CVPR 2009* (pp. 2775–2782). IEEE Conference. <https://doi.org/10.1109/CVPR.2009.5206562>.
- Priestnall, G., Jaafar, J., & Duncan, A. (2000). Extracting urban features from lidar digital surface models. *Computers, Environment and Urban Systems*, 24, 65–78. <http://www.sciencedirect.com/science/article/pii/S0198971599000472>. [https://doi.org/10.1016/S0198-9715\(99\)00047-2](https://doi.org/10.1016/S0198-9715(99)00047-2).
- Python Software Foundation (2017). Python - programming language. <https://www.python.org/>, Accessed date: March 2017.
- Rebelo, C., Rodrigues, A., Tenedório, J., Gonçalves, J., & Marnoto, J. (2015). Building 3d city models: Testing and comparing laser scanning and low-cost uav data using foss technologies. In O. Gervasi, B. Murgante, S. Misra, L. Gavrilova, C. A. Rocha, C. Torre, D. Tanir, & B. Apduhan (Eds.). *Computational Science and Its Applications – ICCSA 2015: 15th International Conference, Banff, AB, Canada, June 22–25, 2015, Proceedings, Part III* (pp. 367–379). Cham: Springer International Publishing. https://doi.org/10.1007/978-3-319-21470-2_26.
- Reilly, C. (2014). Nycitymap & beyond: Nyc building footprints. <https://nycitymap.wordpress.com/2014/12/12/nyc-building-footprints/>, Accessed date: May 2017.
- Rottensteiner, F., & Ch, B. (2002). A new method for building extraction in urban areas from high-resolution lidar data. *(ISPRS) Journal of Photogrammetry and Remote Sensing*, 34, 295–301. <http://www.isprs.org/proceedings/xxiv/part3/papers/paper082.pdf>.
- Santos, T., Rodrigues, A. M., & Tenedório, J. A. (2013). Characterizing urban volumetry using lidar data. *International Archives of the Photogrammetry Remote Sensing and Spatial Information Sciences*. 71–75. <https://doi.org/10.5194/isprarchives-XL-4-W1-71-2013>, Accessed date: May 2016 (Provided by the SAO/NASA Astrophysics Data System).
- Shiravi, S., Zhong, M., & Beykaei, A. S. (2012). Accuracy assessment of building extraction using lidar data for urban planning/transportation applications. *Conference of the Transportation Association of Canada* (pp. 1–15). . <https://doi.org/10.1109/CVPR.2008.4587458>.
- Smith, S., Holland, D., & Longley, P. (2004). The importance of understanding error in lidar digital elevation models. *The International Archives of the Photogrammetry, Remote Sensing and Spatial Information Sciences*, 35, 996–1001.
- Steadman, P., Evans, S., & Batty, M. (2009). Wall area, volume and plan depth in the building stock. *Building Research and Information*, 37, 455–467.
- Truong Pacheco Hong, L., Laefer, D. F., Hinks, T., & Carr, H. (2013). Combining an angle criterion with voxelization and the flying voxel method in reconstructing building models from lidar data. *ComputerAided Civil and Infrastructure Engineering*, 28, 112–129. <https://doi.org/10.1111/j.1467-8667.2012.00761.x>.
- USGS (2014). New York CMGP Sandy 0.7m NPS Lidar. Technical Report United States Geological Survey (USGS) , Accessed date: August 2018.
- Vosselman, G., & Maas, H. (2010). *Airborne and Terrestrial Laser Scanning*. Dunbeath: GBR: Whittles Publishing.
- Wehr, A., & Lohr, U. (1999). Airborne laser scanning introduction and overview. *ISPRS Journal of Photogrammetry and Remote Sensing*, 54, 68–82. <http://www.sciencedirect.com/science/article/pii/S0924271699000118>. [https://doi.org/10.1016/S0924-2716\(99\)00011-8](https://doi.org/10.1016/S0924-2716(99)00011-8).
- Wu, B., Yu, B., Wu, Q., Chen, Z., Yao, S., Huang, Y., & Wu, J. (2017a). An extended minimum spanning tree method for characterizing local urban patterns. *International Journal of Geographical Information Science*, 0, 1–26. <https://doi.org/10.1080/13658816.2017.1384830>.
- Wu, B., Yu, B., Wu, Q., Yao, S., Zhao, F., Mao, W., & Wu, J. (2017b). A graph-based approach for 3d building model reconstruction from airborne lidar point clouds. *Remote Sensing*, 9, 92.
- Yu, B., Liu, H., Wu, J., Hu, Y., & Zhang, L. (2010). Automated derivation of urban building density information using airborne LiDAR data and object- based method. *Landscape and Urban Planning*, 98, 210–219. <https://doi.org/10.1016/j.landurbplan.2010.08.004>, Accessed date: May 2016.
- Yu, B., Liu, H., Wu, J., & Lin, W.-M. (2009). Investigating impacts of urban morphology on spatio-temporal variations of solar radiation with airborne lidar data and a solar flux model: A case study of downtown Houston. *International Journal of Remote Sensing*, 30, 4359–4385. <https://doi.org/10.1080/0143160802555846>.
- Yu, S., Yu, B., Song, W., Wu, B., Zhou, J., Huang, Y., ... Mao, W. (2016). View-based greenery: A three-dimensional assessment of city buildings green visibility using floor green view index. *Landscape and Urban Planning*, 152, 13–26. <http://www.sciencedirect.com/science/article/pii/S0169204616300329>. <https://doi.org/10.1016/j.landurbplan.2016.04.004>.
- Zhou, G., Song, C., Simmers, J., & Cheng, P. (2004). Urban 3d GIS from lidar and digital aerial images. *Computers and Geosciences*, 30, 345–353 Multidimensional geospatial technology for the geosciences.
- Zhou, Q., & Neumann, U. (2008). Fast and extensible building modeling from airborne lidar data. *ACM SIGSPATIAL international conference on advances in geographic information systems (ACM GIS)*.